PHYSICAL REVIEW FLUIDS **7**, 124201 (2022)

Elucidating the oscillation instability of sessile drops triggered by surface acoustic waves

Nicolas Chastrette,[1,2] Michaël Baudoin,[3,4] Philippe Brunet,[2]
Laurent Royon,[5] and Régis Wunenburger[1,*]
[1]*Sorbonne Université, CNRS, Institut Jean Le Rond d'Alembert, F-75005 Paris, France*
[2]*Université de Paris, MSC, UMR 7057, CNRS, F-75013 Paris, France*
[3]*Univ. Lille, CNRS, Centrale Lille, ISEN, Univ. Polytechnique Hauts de France, UMR 8520, IEMN, F-59000 Lille, France*
[4]*Institut Universitaire de France, 1 rue Descartes, 75231 Paris Cedex 05, France*
[5]*Université de Paris, LIED, UMR 8236, CNRS, F-75013 Paris, France*

(Received 23 November 2020; accepted 1 November 2022; published 5 December 2022)

The oscillation instability of sessile drops is ubiquitous in surface acoustic wave (SAW) -powered digital microfluidics. Yet the physics underlying these phenomena has not been elucidated owing to the complex interplay between hydrodynamics, acoustics, and capillarity. We decipher the instability by combining high-speed imaging of the droplet surface vibration with inner acoustic pressure measurements. We rationalize the observed behavior with a model inspired from optomechanics, which couples an intracavity acoustic mode excited by the SAW to a surface deformation eigenmode through amplitude modulation and delayed radiation pressure feedback.

DOI: 10.1103/PhysRevFluids.7.124201

I. INTRODUCTION

Manipulating microparticles, fluids, or soft-matter samples is a key issue in microfluidics, which aims to control physical, chemical, or biological processes at small scales for, e.g., high-throughput screening, bottom-up processing, selectivity or detection sensitivity enhancement, or risk reduction [1]. Among all the available techniques investigated so far, actuation by surface acoustic waves (SAWs) has been early identified as a versatile and efficient tool in both microchannel and drop microfluidics [2–5]. The interaction of a SAW with a sessile drop results in various phenomena depending on the liquid viscosity, drop size, SAW frequency, and phase and intensity distribution: drop trapping [6], oscillations and transport [7–11], liquid atomization [12–16], particle transport or segregation [17,18], mixing [19], and heating [20–22]. The physical mechanisms at play in all these phenomena are all the more difficult to elucidate as they combine acoustics, hydrodynamics, capillarity, and wetting.

In this work, we specifically address the $\sim 10^2$ Hz surface oscillation instability of sessile drops insonicated by $\sim 10^6$ Hz SAWs, a ubiquitous phenomenon which is observed to precede surface wave turbulence [23] as well as two key applications of SAWs in microfluidics, atomization [2,24] and drop transport [9,10], whose elucidation as been quoted as one of the major fundamental challenges in Yeo and Friend's reviews on acoustofluidics [2,3]. The occurrence of oscillations of frequency as low as a few hundreds of Hz in response to MHz acoustic excitation is counterintuitive and suggests that nonlinear mechanisms drive the coupling between acoustics and hydrodynamics.

---

[*] regis.wunenburger@sorbonne-universite.fr

When a SAW irradiates a sessile drop, it is partially converted to a bulk longitudinal wave, which remains confined within the drop acting as a cavity. Here we operate at moderate acoustic excitation frequency $f_{\mathrm{ae}} \simeq 1$ MHz such that $\lambda \simeq R$, where $\lambda = c/f_{\mathrm{ae}}$ is the acoustic wavelength ($c \simeq 1.5\ \mathrm{km\,s^{-1}}$ is the sound velocity in water) and $R \simeq 1.6$ mm the drop radius. This enables us to force a single acoustic mode in the cavity, as opposite to the high-frequency regime ($\lambda \gg R$) in which the high modal density leads to mode overlapping and in turn to chaotic behavior [25]. On the other hand, it has been known since the seminal work of Rayleigh and Lamb that a drop is deformable and displays discrete oscillation eigenmodes, whose behavior is similar to a mechanical oscillator whose stiffness is associated with surface tension and mass to liquid inertia [26,27]. Thus, the oscillation instability observed here couples an intracavity acoustic mode excited by the SAW to discrete surface deformation eigenmodes.

By combining high-speed imaging with acoustic pressure measurements and using an instability model inspired from optomechanics, we demonstrate that drop oscillations result from the mutual interaction between the confined acoustic mode and a single-drop deformation eigenmode through amplitude modulation and delayed radiation pressure feedback. Interestingly, this scheme is reminiscent of the parametric instability of gravitational wave interferometric detectors [28], force-sensing microlevers [29,30], and opto-mechanical oscillators designed for quantum intrication [31].

The article is organized as follows. In Sec. II we describe the experimental setup and protocol (complementary information is provided as Supplemental Material). In Sec. III we characterize the forced acoustic cavity mode. In Sec. IV we evidence and characterize the oscillation instability. Finally, in Sec. V we model the instability.

II. EXPERIMENTAL SETUP

A sessile water drop of volume $V = 10.0\ \mu\mathrm{l}$ is deposited on a 10-mm-thick glass slab using a precision micropipette. The drop partially wets the slab with a contact angle θ_{w} close to 90° and a contact line radius $R_w = 1.65$ mm defined in Fig. 1. The drop is irradiated by a plane, progressive Rayleigh wave with frequency $f_{\mathrm{ae}} = 0.84$ MHz, which is generated by mode conversion using a broadband custom Imasonic contact longitudinal transducer mounted on an Olympus ABWX-2001 variable-angle plexiglas wedge, as sketched in Fig. 1. Since the ratio of substrate thickness over Rayleigh wavelength is approximately equal to three, guided waves are practically pure surface (Rayleigh) waves, according to [32]. The slab edges are surrounded by PDMS, which ensures efficient attenuation of SAW echoes in the glass slab. The tip of a Precision Acoustics needle hydrophone with 200 μm-diameter active element is put in contact with the liquid, allowing us to measure the intracavity acoustic pressure. Full pictures of the drop are acquired using a IDS Imaging camera at 30 frames per second (fps), from which the height of the drop apex H is monitored during the whole evaporation process. The oscillations of the drop-free surface in a narrow field close to its apex, shown in Fig. 1, are recorded at 1000 fps with a 2.2 μm/pixel resolution using a Photron SA-5 high-speed camera equipped with a zoom lens (Navitar ×40 objective).

Basically, the experiments consist in exciting the drop with a harmonic SAW at carrier frequency f_{ae} close to one of the resonance frequencies f_{ar} of the acoustic cavity formed by the drop. Amplitude ramps are applied in order to detect the onset of the surface oscillation instability as function of the drop volume. Complementary details about the experimental setup and timescales are given in [33].

III. THE DROP AS AN ACOUSTIC CAVITY

First, the linear acoustic response of the cavity formed by the drop is determined by supplying the transducer with a voltage signal $u(t)$ whose frequency linearly sweeps over the range 0.8–0.9 MHz, with low amplitude $U = 5$ V and 20 ms duration, while the intracavity pressure $p(t)$ is recorded. The spectral amplitude $|u(f)|$ of $u(t)$ is displayed in Fig. 2(a). The spectral amplitude $\hat{P}(f) = |p(f)/u(f)|$ of the pressure response of a freshly deposited drop (height $H_0 = 1.72$ mm)

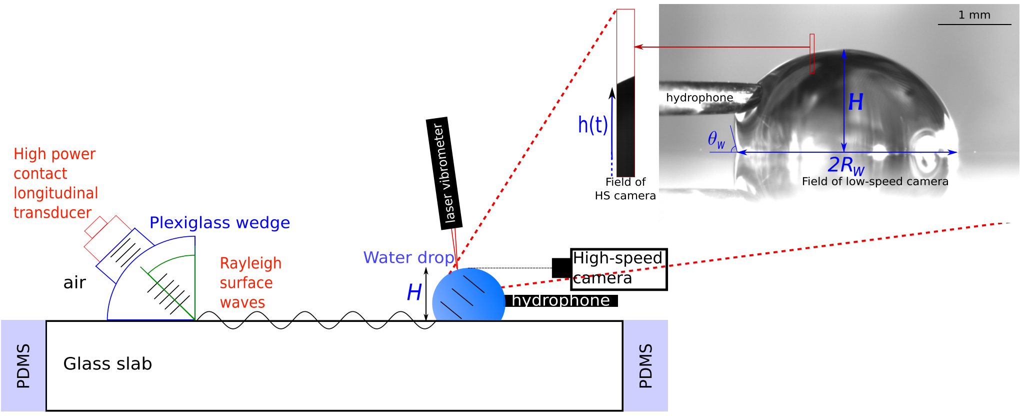

FIG. 1. Sketch of the experimental setup. A 10.0 μl water drop deposited on a glass slab is irradiated with a harmonic progressive Rayleigh wave generated using a contact longitudinal transducer mounted on a wedge. The slab edges are surrounded by PDMS, which ensures efficient attenuation of SAW echoes in the glass slab. A needle hydrophone, whose tip is brought into contact with the liquid surface, measures the intracavity pressure. Full pictures of the slowly evaporating drop are taken at 30 fps using a camera (main picture at top right of the figure), while the oscillations of the drop-free surface in a narrow field close to its apex (red frame on the picture) are recorded at 1000 fps using a high-speed camera (narrow picture on the left of the main picture). A laser vibrometer pointing close to the apex is used for measuring low-amplitude surface oscillations in independent experiments dedicated to the characterization of the unstable surface eigenmode, which are presented in [33].

is shown in Fig. 2(a), where $p(f)$ is the Fourier transform of $p(t)$. $\hat{P}$ exhibits two peaks in the range 0.8–0.9 MHz respectively at $f_{\mathrm{ar}} \simeq 0.81$ MHz and $f'_{\mathrm{ar}} \simeq 0.87$ MHz. Considering the drop as hemispherical and assuming (1) no displacement of the rigid glass surface (hereinafter called equatorial plane) and (2) pressure node at the drop-free surface, the acoustic eigenmodes can be expressed using spherical waves [34]. Their eigenfrequencies $f_{\ell,q}$ satisfy $j_\ell(2\pi R f_{\ell,q}/c) = 0$ where $R = [3V/(2\pi)]^{1/3} = 1.68$ mm, with j_ℓ the spherical Bessel function of the first kind, ℓ a positive integer, and q the number of the root of j_ℓ in ascending order [33]. Two eigenfrequencies $f_{2,1} = 0.82$ MHz (corresponding to three degenerate modes symmetrical to the equatorial plane, labeled by $m = 0, \pm 2$ [33]) and $f_{0,2} = 0.89$ MHz fall in the range 0.8–0.9 MHz and are found to be close to the measured peak frequencies f_{ar} and f'_{ar}. This demonstrates that these peaks do correspond to the resonant forcing of cavity eigenmodes.

Due to evaporation, the height H of the drop apex decreases in time while its contact line remains pinned during the first 5 min, resulting in a continuous increase of f_{ar}; see Figs. 2(a) and 2(b). A numerical calculation (using Comsol software) of the acoustic eigenmodes of a sessile drop with variable height H, fixed R_w, initial volume V, and initial height H_0 evidences that, when the drop is not hemispherical ($H \neq R_w$), the eigenfrequencies of the ($\ell = 2, q = 1$) modes split [33]. The comparison between the variations of f_{ar} with H measured during several experiments and the computed variations of the eigenfrequencies of the $m = \pm 2$ and $m = 0$ modes vs H, shown in Fig. 2(b), allows us to unambiguously identify f_{ar} as the resonance frequency of the ($\ell = 2, q = 1, m = \pm 2$) modes, whose pressure field distribution is shown in inset of Fig. 2(b).

As shown in Fig. 2(a), during evaporation the cavity pressure response is accurately described by a one-dimensional (1D) resonator model:

$$\hat{P}(f) = \hat{P}_{\mathrm{i}} \left| 1 + \left[1 - \frac{\pi}{2Q_{\mathrm{ar}}} \exp\left(i\pi \frac{f}{f_{\mathrm{ar}}} \right) \right] \right|^{-1}, \tag{1}$$

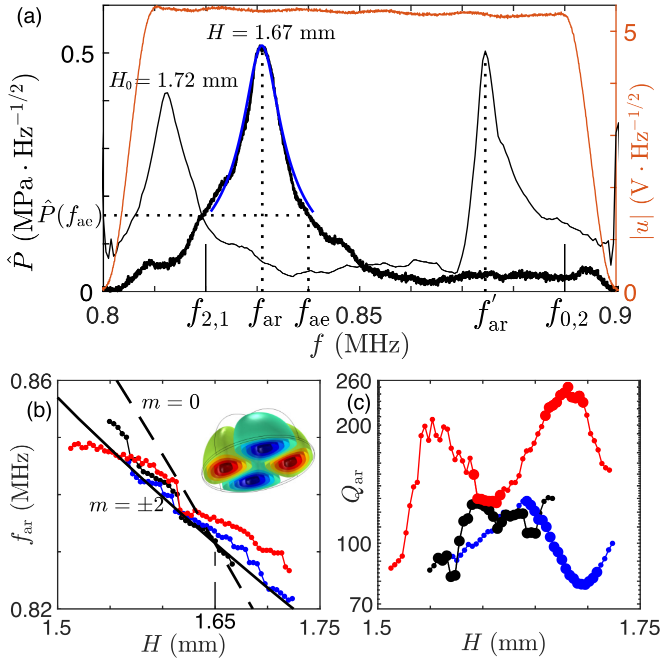

FIG. 2. (a) Red curve: Narrow-band spectrum $|u(f)|$ of the frequency-swept voltage periodically applied to the transducer to scan the drop acoustic resonances during its evaporation. Spectrum $\hat{P}(f) = |p(f)/u(f)|$ of the drop pressure response immediately after its deposition (thin black curve) and after 3 min of evaporation (bold black curve). Blue curve: best fit by Eq. (1). $f_{2,1}$ and $f_{0,2}$ are the numerically predicted acoustic eigenfrequencies of a hemispherical drop with radius $R = 1.68$ mm. (b) Acoustic resonance frequency f_{ar} vs drop height H during the evaporation of three drops (connected red, black, and blue symbols). Solid and dashed curves: theoretical predictions; see text. Inset: Pressure distribution of the forced $m = \pm 2$ eigenmodes. (c) Corresponding acoustic quality factor Q_{ar}. Bold symbols: measurements during which the oscillation instability is observed.

where $\hat{P}_i = (3.5 \pm 1.5)\,\mathrm{kPa\,V^{-1}}$ is the magnitude related to the excitation of the acoustic wave injected into the drop by mode conversion of the leaky SAW and Q_{ar} is the quality factor, whose value is determined by fitting Eq. (1) to the resonance peak. Figure 2(c) displays the variations of Q_{ar} vs H measured over several experiments. Its fluctuations lie in the range 80–250. Its dispersion may be ascribed to the slight variations of the shape of the triple lines along the substrate and the needle tip from one experiment to another, while its variations during evaporation may be ascribed to the evolving drop shape.

IV. OSCILLATION INSTABILITY

We now address the oscillation instability. Due to evaporation, f_{ar} increases at a typical rate of $3.5\,\mathrm{kHz\,min^{-1}}$. Instead of continuously adjusting the frequency f_{ae} of the acoustic excitation for maintaining the same interference conditions in the drop, we set f_{ae} slightly above the initial value of f_{ar} [see Fig. 2(a)] $f_{ae} = 0.84$ MHz. Hence, f_{ar} crosses f_{ae} after 3–4 min and the drop acoustic resonance is scanned in 5 min, which leads us to analyze how the drop unstable behavior changes with time. Accordingly, every 15 s, (1) the linear acoustic response of the cavity is measured as described in Sec. III [see inset in Fig. 3(a), (2) then the drop is insonicated using a harmonic SAW with fixed frequency f_{ae}, amplitude U increasing as $\sqrt{t}$ from 0 to 55 V in 1 s, as sketched in Fig. 3(a), so that the radiation pressure (RP) exerted by the intracavity acoustic field on the drop surface,

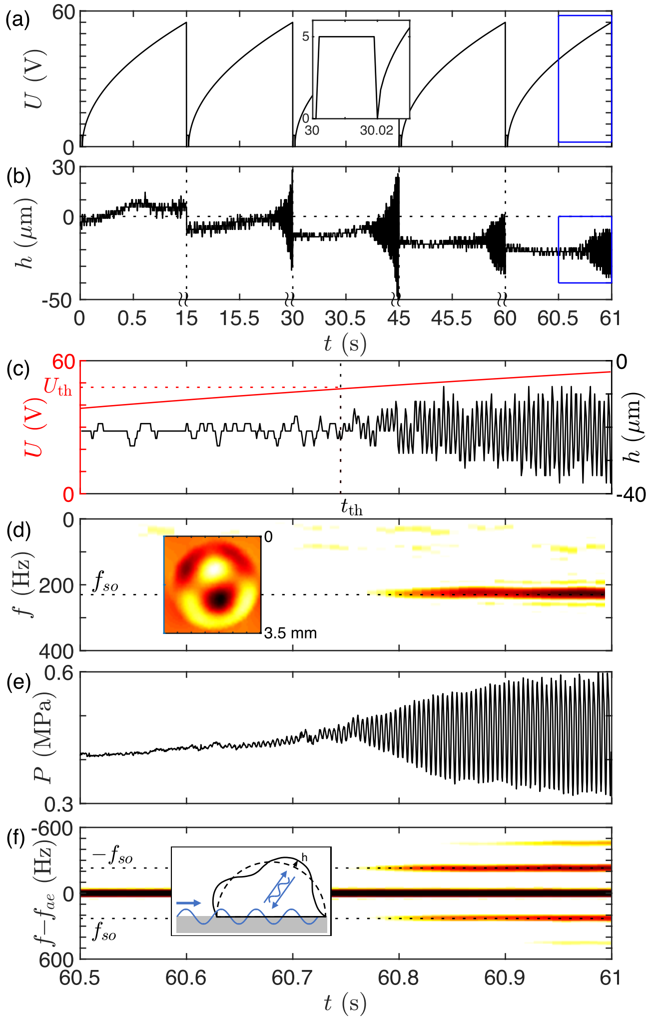

FIG. 3. (a) Amplitude $U(t)$ of the sine voltage signal prescribed to the transducer, which is 15 s-periodic, 1 s-long (note the breaks on timescale). Inset: Zoom on the frequency-swept, small-amplitude signal used to assess the cavity acoustic response. (b) Relative height $h(t)$ (arbitrary origin) of the drop surface imaged using the high-speed camera, undergoing a slow decrease due to evaporation and possibly oscillations during excitation. (c) Enlargements of the parts of the signals framed in blue in (a) and (b), evidencing the surface oscillation instability triggered for $U \geqslant U_{\mathrm{th}}$ starting from t_{th}. (d) Spectrogram of $h(t)$ evidencing a monochromatic oscillation at frequency $f_{\mathrm{so}} \simeq 230$ Hz. Inset: Corresponding drop deformation pattern independently measured from above [33]. (e) Amplitude $P(t)$ of the intracavity pressure $p(t)$, displaying modulation starting from t_{th}. (f) Spectrogram of p showing the appearance of satellite peaks shifted from the carrier frequency f_{ae} by $\pm f_{\mathrm{so}}$ starting from t_{th}. Inset: Sketch of the feedback of the drop deformation on the intracavity field.

which is proportional to U^2, increases linearly in time, (3) while $p(t)$ and the drop surface height $h(t)$, defined in Fig. 1 and shown in Fig. 3(b), are recorded, (4) the remaining time is dedicated to data transfer.

As can be understood from Fig. 2(a), during evaporation, starting from nonresonant conditions ("blue detuning" in optical physics), the drifting resonance frequency f_{ar} crosses f_{ae} for a given height $H_{\mathrm{res}} \simeq 1.63$ mm, realizing a resonant forcing. When f_{ar} overruns f_{ae}, the cavity is driven

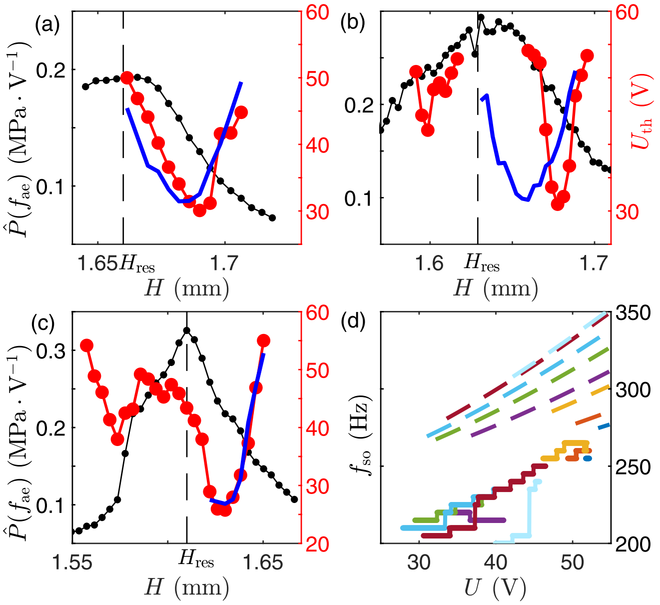

FIG. 4. (a)–(c) Left scale, joined black symbols: H-dependent pressure response $\hat{P}$ at excitation frequency $f_{\rm ae}$. Right scale, joined red symbols: instability threshold voltage $U_{\rm th}$ vs H. Blue curve: best fit of $U_{\rm th}(h)$ by Eqs. (4) and (6). (d) Solid curves: measured surface oscillation frequency $f_{\rm so}$ vs U ($\geqslant U_{\rm th}$) for several values of H. Dashed curves: corresponding predictions from Eq. (7).

away from resonance ("red detuning"). Accordingly, as shown in Figs. 4(a)–4(c), when H decreases, the magnitude of the intracavity pressure response to excitation $\hat{P}(f_{\rm ae})$ first increases, then reaches a maximum when $f_{\rm ar} = f_{\rm ae}$, and finally decreases. The effect of the evaporation on the drop eigenmode excitation and the way to take advantage of it are reminiscent of a previous study of concentration patterns of colloids in SAW-excited drops [35].

Meanwhile, as shown in Figs. 3(b) and 3(c), h slowly decreases due to evaporation and undergoes oscillations during excitation when U exceeds a threshold $U_{\rm th}$. The variations of $U_{\rm th}$ vs H, measured during several experiments, some of which displayed in Figs. 4(a)–4(c), reveal that two instability tongues reproducibly show up on the right-hand side ($f_{\rm ae} > f_{\rm ar}$) and left-hand side ($f_{\rm ae} < f_{\rm ar}$) of the peak on the curve of variation of $\hat{P}(f_{\rm ae})$ vs H, demonstrating that the instability onset depends on the acoustic interference conditions and the instability occurs close to (and not at) an eigenfrequency of the acoustic cavity. Also, Fig. 2(c) shows that the occurrence of the instability is not correlated to the variations of $Q_{\rm ar}$.

The spectrogram of $h(t)$ shown in Fig. 3(d) evidences that, at the instability onset, h shows harmonic oscillations of frequency $f_{\rm so} \simeq 230$ Hz. An independent recording of the deformations of the image of a grid visualized through the drop [33] allowed us to measure the free-surface deformations and to identify the corresponding forced surface eigenmode, whose experimental pattern is shown in inset of Fig. 3(d) [33,36]. We conclude that the instability involves a single surface deformation eigenmode.

V. MECHANISM OF INSTABILITY

To gain insight into the instability mechanism, we consider the time evolution of the magnitude P of $p(t)$, shown in Fig. 3(e). P smoothly increases with U up to the instability threshold. Once the surface oscillates, P exhibits oscillations at the frequency of the drop surface oscillations $f_{\rm so}$ and whose amplitude increases with U.

A. Amplitude modulation of the intracavity field by surface oscillations

This amplitude modulation of $p(t)$ can be explained as follows: the drop behaves as a 1D resonator with an effective length modulated by the free surface oscillations $h(t) = A\cos(\omega_{\mathrm{so}} t)$ with $\omega_{\mathrm{so}} = 2\pi f_{\mathrm{so}}$; see inset in Fig. 3(f). Hence, f_{ar} is modulated at frequency f_{so} with amplitude $A\frac{df_{\mathrm{ar}}}{dh}$, where $\frac{df_{\mathrm{ar}}}{dh}$, which quantifies the sensitivity of f_{ar} to drop deformations, is always negative since a 1D resonator eigenfrequency decreases with its length. Since the delay of adaptation of intracavity pressure $p(t)$ to variations of interference conditions $\tau_{\mathrm{ar}} = Q_{\mathrm{ar}}/\omega_{\mathrm{ar}} \simeq 20\,\mu\mathrm{s}$ is much shorter than the period of these variations $f_{\mathrm{so}}^{-1} \simeq 4$ ms, $P(t)$ quasistatically follows these variations and in turn adopts a similar modulation at frequency f_{so}, with amplitude $\Delta P = U\,\frac{\partial \hat{P}}{\partial f_{\mathrm{ar}}}(f_{\mathrm{ae}})A\frac{df_{\mathrm{ar}}}{dh}$. This is experimentally confirmed by the spectrogram of $p(t)$ shown in Fig. 3(f), which displays at $\Delta P/P \ll 1$ a single pair of satellite peaks shifted from f_{ae} by $\pm f_{\mathrm{so}}$, a signature of amplitude modulation at frequency f_{so} [33].

B. Feedback of the amplitude-modulated intracavity field on surface oscillations

Now we consider the feedback of the amplitude-modulated intracavity field on surface oscillations. This feedback is provided by the radiation pressure exerted by the intracavity acoustic field on the drop surface. Radiation pressure, which is the time average over f_{ae}^{-1} of the pressure $p(t)$ exerted on the drop-free surface, is a normal stress oriented outwards whose magnitude Π satisfies in order of magnitude

$$\Pi = P^2/(\rho c^2), \tag{2}$$

where ρ is water density [37,38]. As a consequence, the intracavity pressure modulation (with amplitude ΔP) induced by the surface oscillations results in radiation pressure oscillations of amplitude $\Delta\Pi = 2P\,\Delta P/(\rho c^2)$ at instability onset, which have therefore the same frequency f_{so} as the surface oscillations. These radiation pressure oscillations may damp or amplify the surface oscillations depending on their phase difference, as analyzed hereinafter.

Close to resonance, the amplitude h of the surface eigenmode forced by radiation pressure oscillations follows the dynamics of a forced mass-spring system: $\ddot{h} + \frac{\omega_{\mathrm{so}}}{Q_{\mathrm{so}}}\dot{h} + \omega_{\mathrm{so}}^2 h = \frac{F(h)}{m}$, where $\dot{h}$ is the time derivative of h and $Q_{\mathrm{so}} = (40 \pm 15)$ is the independently measured quality factor of the resonance of the surface eigenmode [33]. Evaluating the effective wave number of the surface eigenmode as $k_{\mathrm{so}} = \frac{4}{R}$ [33], $F \propto k_{\mathrm{so}}^{-2}\Delta\Pi$ is the modulated acoustic radiation force exerted on a portion of drop surface of characteristic size equal to one deformation wavelength $\lambda_{\mathrm{so}} = 2\pi/k_{\mathrm{so}}$ and $m \propto \rho k_{\mathrm{so}}^{-3}$ the corresponding mass of moving water. At the instability onset, we can linearize the variations of F around equilibrium: $\frac{F(h)}{m} = \frac{K_{\mathrm{a}}}{m}h$ where $K_{\mathrm{a}} = F'(0)$. Thus, h satisfies

$$\ddot{h} + \frac{\omega_{\mathrm{so}}}{Q_{\mathrm{so}}}\dot{h} + \left(\omega_{\mathrm{so}}^2 - \frac{K_{\mathrm{a}}}{m}\right)h = 0, \tag{3}$$

where

$$\frac{K_{\mathrm{a}}}{m} = \frac{k_{\mathrm{so}}}{\rho^2 c^2}U^2\,\hat{P}\,\frac{\partial \hat{P}}{\partial f_{\mathrm{ar}}}(f_{\mathrm{ae}})\,\frac{df_{\mathrm{ar}}}{dh} \tag{4}$$

within an unknown factor. Note that K_{a} accounts for a change in the surface stiffness $m\omega_{\mathrm{so}}^2$ (“acoustic spring”) induced by radiation pressure [39].

C. Delayed radiation pressure feedback as a plausible origin of the instability

1. Case $H > H_{res}$ (early stage of evaporation)

First, we focus on the case $H > H_{\mathrm{res}}$ encountered at the early stage of evaporation, which corresponds to the right-hand side of the peak of the $\hat{P}(f_{\mathrm{ae}})$ vs H curves shown in Figs. 4(a)–4(c) and where $f_{\mathrm{ae}} > f_{\mathrm{ar}}$ (domain of blue detuning). In this domain, a decrease of f_{ar} due to a crest ($h > 0$)

moves $f_{\rm ar}$ away from $f_{\rm ae}$ and thus detunes the cavity, resulting in $\frac{\partial \hat{P}}{\partial f_{\rm ar}}(f_{\rm ae}) > 0$ and hence $K_{\rm a} < 0$. According to Eq. (3), the surface eigenmode dynamics is that of a stiffer yet damped free harmonic oscillator exhibiting no instability. To explain the oscillation instability, a key point is to consider the finite delay $\tau_{\rm ar}$ of adaptation of P, and hence of Π, to the variations of the intracavity interference conditions caused by the surface oscillations at pulsation ω. In the harmonic regime, this results in a phase lag of F with respect to h. With the convention that the actual harmonic surface deformation is the real part of $h = H\exp(i\omega t)$, $K_{\rm a}$ has to be changed to $K_{\rm a}\exp(-i\phi)$ in Eq. (3), where $\phi > 0$ and $\phi = \omega\tau_{\rm ar} \simeq \omega_{\rm so}\tau_{\rm ar} \simeq 0.03 \ll 1$. Noting that in harmonic regime $i\omega h = \dot{h}$, h satisfies

$$\ddot{h} + \left(\frac{\omega_{\rm so}}{Q_{\rm so}} + \frac{K_{\rm a}}{m\omega}\sin\phi\right)\dot{h} + \left(\omega_{\rm so}^2 - \frac{K_{\rm a}}{m}\cos\phi\right)h = 0. \tag{5}$$

Since $\sin\phi > 0$ and $K_a < 0$, the damping term in Eq. (5) is reduced by the delayed radiation pressure feedback. The condition for instability is a negative damping occurring for $U \geqslant U_{\rm th}$ such that

$$\frac{|K_{\rm a}(U_{\rm th})|}{m} = \frac{\omega_{\rm ar}\omega_{\rm so}}{Q_{\rm ar}Q_{\rm so}} \tag{6}$$

given $\omega \simeq \omega_{\rm so}$ and $\sin\phi \simeq \phi$. Furthermore, as shown by Eq. (5), the acoustic spring results in an increase of the surface oscillation frequency $\omega'_{\rm so}$ with respect to its natural value $\omega_{\rm so}$:

$$\omega'_{\rm so} = \sqrt{\omega_{\rm so}^2 - \frac{K_{\rm a}}{m}} \tag{7}$$

since $\cos\phi \simeq 1$.

The instantaneous oscillation frequency $f'_{\rm so}$ is extracted from the spectrograms of $h(t)$ measured for several values of H. Figure 4(d) evidences the increase of $f'_{\rm so}$ with U, which is in agreement with the stiffening predicted by Eq. (7). The negative offset of $f'_{\rm so}$ with respect to $f_{\rm so} = 230$ Hz may be ascribed to the radiation pressure-induced static deformation of the drop; see [33]. To test the quantitative validity of this model for $f_{\rm ae} > f_{\rm ar}$, we compare Eqs. (6) and (7) to the experimental data using Eq. (1) fitted to the resonance curve at each value of H, Eq. (4), and $Q_{\rm ar} = 100$, α, defined as $\frac{df_{\rm ar}}{dh} = -\alpha\frac{f_{\rm ar}}{H}$, being the only fitting parameter. As shown in Figs. 4(a)–4(c), the measured and predicted instability tongues $U_{\rm th}(H)$ are in quantitative agreement. The same goes for the measured and predicted rates of variation of $f'_{\rm so}(U)$, as shown in Fig. 4(d). Moreover, the values of α corresponding to the best fits of $U(H)$ and of the rates of variation of $f_{\rm so}(U)$ are scattered in a narrow range (between 2×10^{-4} and 10^{-3}). Thus, the proposed model reproduces quantitatively and self-consistently two main observables of the instability for $H > H_{\rm res}$, namely, its threshold and the radiation pressure-induced stiffening.

2. Case $H < H_{res}$ (late stage of evaporation): Taking the static drop deformation into account

Finally, we consider the case $H < H_{\rm res}$ encountered at the late stage of evaporation, which corresponds to the left-hand side of the peak of the $\hat{P}(f_{\rm ae})$ vs H curve shown in Figs. 4(a)–4(c) and where $f_{\rm ae} < f_{\rm ar}$ (domain of red detuning). In this domain, $\frac{\partial \hat{P}}{\partial f_{\rm ar}}(f_{\rm ae}) < 0$ and hence $K_a > 0$. As a consequence, the delayed radiation pressure feedback *increases* the damping term in Eq. (5). Thus, according the aforementioned proposed instability mechanism, no oscillation instability should be observed in the domain of red detuning. To explain the puzzling observation of oscillations in this domain, it is necessary to consider another effect of radiation pressure, which is the static deformation of the drop.

To evidence this effect, U is increased as $\sqrt{t}$ from 25 to 55 V in order to vary radiation pressure as quasistatically as possible. For $H = H_1 > H_{\rm res}$ and $H = H_2 > H_{\rm res}$ as defined in Fig. 5(a), we observe in Figs. 5(b) and 5(c) that when U increases in time, the magnitude of the pressure response of the cavity P/U monotonously decreases with time outside oscillatory episodes. For $H = H_3 \lesssim H_{\rm res}$, we observe in Fig. 5(d) that when U increases, P/U increases, then decreases

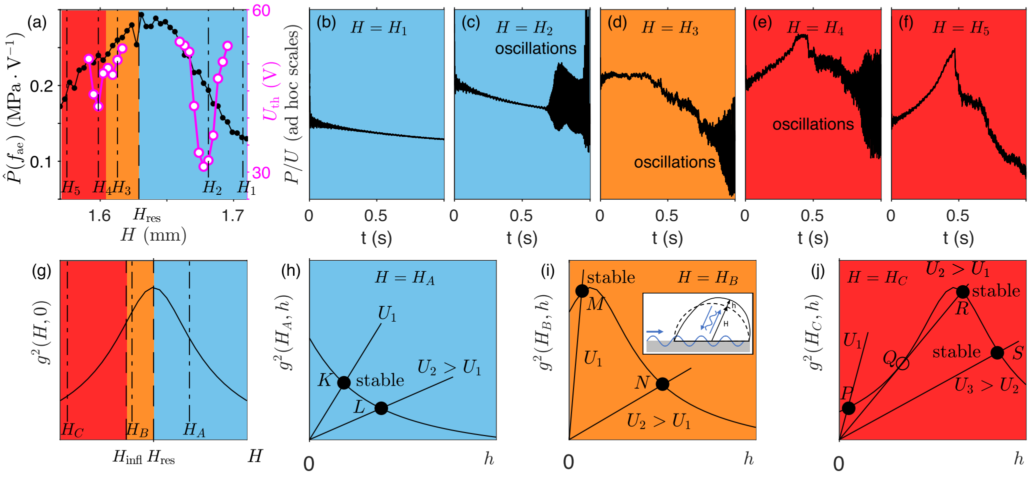

FIG. 5. (a) Left scale, joined black symbols: H-dependent pressure response $\hat{P}$ at excitation frequency f_{ae}. Right scale, joined open magenta symbols: instability threshold voltage U_{th} vs H. The blue area corresponds to $H > H_{res}$ (blue detuning). The orange and red areas correspond to $H < H_{res}$ (red detuning). (b–f) Time evolution of the cavity pressure response $P/U = \hat{P}$ during a U ramp for four different values of the drop height $H = H_i$, $i = 1$ to 4, as defined in (a). Oscillation episodes are visible in (c)–(e). (g) Schematic variation of the square of the pressure response $\hat{P}^2 = P^2/U^2 = g^2$ vs H. (h–j) Schematic variation of g^2 vs resonator lengthening h [see inset of (i)] for three different values of the drop height $H = H_X$, $X = A, B, C$, as defined in (g). Inset of (i): Sketch of the drop quasistatic deformation.

outside the oscillatory episode. Finally, for $H = H_4 \ll H_{res}$ and $H = H_5 \ll H_{res}$, we observe in Figs. 5(e) and 5(f) that when U increases, P/U increases, then encounters a jump, then decreases outside oscillatory episodes. This U dependence of $P/U = \hat{P}$ is not described by Eq. (1), which states that $\hat{P}(f_{ae})$ depends only on H (which determines f_{ar}), i.e., should be independent of U outside oscillatory episodes. To explain this observation, we have to take into account that, in addition to oscillating, the irradiated drop is quasistatically deformed by radiation pressure, which modifies the interference conditions in the drop exhibiting the oscillation instability. Such a static nonlinear behavior has been already observed and modeled by Issenmann *et al.* [40] in the case of a liquid surface constituting one end of a near-1D acoustic cavity. In what follows, we show that the model of Ref. [40] applies to our experimental results, allowing us to explain why oscillations are observed in the domain of red detuning.

Under the effect of quasistatic radiation pressure, the irradiated drop indeed undergoes a small, tridimensional (3D), quasistatic deformation with respect to its hemispheric base shape, as sketched in inset of Fig. 5(i). This deformation is determined by the spatial distribution of the intracavity acoustic field, the constraints of droplet volume conservation and that of pinned contact line. Although this deformation is perceptible in the full pictures of the droplet, its 3D shape and its small amplitude discouraged us from monitoring it. On the one hand, at steady state, the drop surface curvature κ satisfies $\Pi \sim \gamma \Delta\kappa$, where γ is water surface tension and $\Delta\kappa = \kappa - 2/R$ is the curvature perturbation of the drop. For small deformations, linearization of κ with respect to the drop deformation leads to $\Delta\kappa \sim \gamma h/R^2$, where h stands for the quasistatic increase h of the effective length of the 1D resonator describing the behavior of the acoustic cavity. Finally, owing to Eq. (2), $P^2 \simeq K\frac{\gamma\rho c^2}{R^2}h$, where K is a dimensionless factor, or equivalently

$$\frac{P^2}{U^2} \simeq \frac{K\gamma\rho c^2}{R^2U^2}h. \qquad (8)$$

On the other hand, the quasistatic increase of the resonator length h leads to a quasistatic decrease of the cavity resonance frequency f_{ar}. Defining $g(H,h)$ as $g(H,h) = \hat{P}_{\mathrm{i}}|1+[1-\frac{\pi}{2Q_{\mathrm{ar}}}\exp(i\pi\frac{f_{\mathrm{ae}}}{f_{\mathrm{ar}}(H+h)})]|^{-1}$, we rewrite Eq. (1) expressed for $f = f_{\mathrm{ae}}$ as

$$\frac{P^2}{U^2} = g^2(H,h). \tag{9}$$

For given values of H and U, h corresponds to the stable working point of the nonlinear system described by Eqs. (8) and (9). As illustrated in Figs. 5(g)–5(j), h can be graphically determined as the abscissa of the intersection point of the line $h \mapsto \frac{K\gamma\rho c^2}{R^2U^2}h$, whose slope decreases when U increases, and of the curve $h \mapsto g^2(H,h)$, which is invariant with respect to U variations. Now we can examine the three possible cases. (1) As shown in Fig. 5(h), for $H = H_A > H_{\mathrm{res}}$, when U increases from U_1 to U_2, g^2, hence P/U, monotonously decrease from K to L. This qualitatively describes the observed behavior of P/U for $H = H_1 > H_{\mathrm{res}}$ and $H = H_2 > H_{\mathrm{res}}$ shown in Figs. 5(b) and 5(c), respectively. (2) Defining H_{infl} as the abscissa of the left-hand inflection point of the $h \mapsto g^2(H,0)$ curve shown in Fig. 5(g), as shown in Fig. 5(h), for $H = H_B$ such that $H_{\mathrm{infl}} > H_B > H_{\mathrm{res}}$, when U increases from U_1 to U_2, g^2 continuously increases, then decreases from M to N. This qualitatively describes the observed behavior of P/U for $H = H_3 \lesssim H_{\mathrm{res}}$ shown in Fig. 5(d). (3) As shown in Fig. 5(j), for $H = H_C < H_{\mathrm{infl}}$, when U increases from U_1 to U_2, g^2 increases from P to Q where it loses its stability and then jumps to R. When U further increases from U_2 to U_3, g^2 continuously decreases from R to S. This qualitatively describes the observed behavior of P/U for $H = H_4$ and $H = H_5$ shown in Figs. 5(e) and 5(f). The only qualitative difference between experiment and model is the jump which is experimentally observed to be negative whereas it is theoretically predicted to be positive. This may be ascribed to a possible drop of the cavity quality factor when the drop discontinuously changes its shape, a 3D effect that is not taken into account in the 1D model. We conclude to a qualitative agreement between the model and the observed quasistatic behavior of the cavity.

Now, the model can be used to explain why the oscillation instability was observed for $H < H_{\mathrm{res}}$. As illustrated in Figs. 5(b)–5(f), oscillations are actually observed only when P/U decreases with U, H being larger or smaller than H_{res}. According to the model, this is due to a cavity lengthening such that the stable working point of the acousto-mechanical system is always located on a decreasing part of the $h \mapsto g^2(H,h)$ curve; see Figs. 5(h)–5(j). As a result, regardless of the value of H and in particular for $H < H_{\mathrm{res}}$, oscillations only occur when $\frac{d\hat{P}}{dh} < 0$. Since $\frac{d\hat{P}}{dh} = \frac{d\hat{P}}{df_{\mathrm{ar}}}\frac{df_{\mathrm{ar}}}{dh}$ and $\frac{df_{\mathrm{ar}}}{dh} < 0$, this leads to the necessary condition $\frac{d\hat{P}}{df_{\mathrm{ar}}} > 0$, i.e., to $K_a < 0$, which is precisely the situation in which delayed feedback is able to trigger the oscillation instability. In other words, the phenomenon of radiation pressure-induced static drop deformation brings red-detuned drops, drops such that $H < H_{\mathrm{res}}$, into states of blue detuning, i.e., such that their static length $H + h$ satisfies $(H + h) > H_{\mathrm{res}}$, in which the oscillation instability can be triggered.

To conclude this part, we succeeded in explaining the underlying mechanism of oscillation instability and the occurrence of both instability tongues by combining a model of instability triggered by amplitude modulation and delayed radiation pressure feedback and a nonlinear model of static drop deformation by radiation pressure.

VI. DISCUSSION

Since acoustic streaming results in stresses exerted by the intracavity acoustic field on the drop surface that add to radiation pressure, it may also be considered as possibly intervening in the instability mechanism. However, at the frequency investigated here ($f_{\mathrm{ac}} \sim 1$ MHz), the acoustic attenuation length L_a is of the order of 50 m, i.e., it is 3×10^4 larger than the drop radius R. Hence the wave attenuation in the drop is extremely small, in contrast to experiments performed at higher frequencies ($f_{\mathrm{ac}} \sim 50$ MHz) reported in the literature where $L_a/R \sim 10$ and where acoustic streaming effects were evidenced. Therefore, we confidently assume that radiation pressure is the dominant phenomenon intervening in the instability mechanism.

We note that the phase-locking mechanism proposed in [41,42] for explaining the instability of low-frequency surface eigenmodes ($f_{\mathrm{so}} \ll f_{\mathrm{ar}}$) predicts that (1 the components along the liquid surface of the acoustic and surface eigenmodes coincide and (2) the larger the acoustic amplitude, the larger the amplitude of the surface oscillation. On the contrary, we observed that the symmetries of the acoustic and surface eigenmodes did not coincide [see Figs. 3(d) and 2(b)] and that the oscillation amplitude depends also on the droplet height, thus making the phase-locking mechanism inadequate for explaining our observations, possibly because it does not take into account the feedback of the drop shape on the acoustic field.

In the light of these results, our conjecture is that SAW-driven surface turbulence [23] may originate from the independent excitation of numerous surface eigenmodes above different thresholds since many surface eigenmodes can in principle interact with the intracavity acoustic field, as shown in [33]. Moreover, we note that the contact-line pinning, which usually hinders drop transport, can be overcome by low-frequency drop oscillations [10,11], thus making of this oscillation instability an essential ingredient of SAW-induced transport. Indeed, since intracavity resonances are expected to persist up to 40 MHz [9], we expect the above unraveled instability mechanism to hold in the higher frequency range where drop transport is usually achieved, possibly cooperating with acoustic streaming. Finally, the instability can be also triggered by a hybrid combination of surface and bulk waves [32] and is therefore generic, as shown by the experiments dedicated to the imaging of the drop surface deformations presented in [33].

ACKNOWLEDGMENTS

M.B. first observed the phenomenon. R.W. proposed and designed the experiments and supervised the project. N.C. built the setups and carried out the experiments and their analysis. P.B. and M.B. provided experimental support and advice. M.B. performed the numerical computations. All authors contributed to the interpretation of the results. R.W. proposed and derived the model and wrote the manuscript. M.B. and P.B. helped shape the research and manuscript. The authors thank J. L. Thomas, A. Riaud, and O. Bou-Matar for their help in the use of their vibrometer, J. Marchall for his help in instrumentation, and J. L. Thomas, J. Pierre, and A. Bussonnière for helpful advice.

---

[1] P. Tabelling, *Introduction to Microfluidics* (Oxford University Press, Oxford, 2005).

[2] J. Friend and L. Y. Yeo, Microscale acoustofluidics: Microfluidics driven via acoustics and ultrasonics, Rev. Mod. Phys. **83**, 647 (2011).

[3] L. Yeo and J. Friend, Surface acoustic wave microfluidics, Annu. Rev. Fluid Mech. **46**, 379 (2014).

[4] W. Connacher, N. Zhang, A. Huang, J. Mei, S. Zhang, T. Gopesh, and J. Friend, Micro/nano acoustofluidics: Materials, phenomena, design, devices and applications, Lab Chip **18**, 1952 (2018).

[5] A. Riaud, M. Baudoin, J.-L. Thomas, and O. Bou Matar, Saw synthesis with IDTs array and the inverse filter: Toward a versatile saw toolbox for microfluidics and biological applications, IEEE Trans. Ultrason. Ferroelect. Freq. Contr. **63**, 1601 (2016).

[6] M. Alvarez, J. Friend, and L. Yeo, Surface vibration induced spatial ordering of periodic polymer patterns on a substrate, Langmuir **24**, 10629 (2008).

[7] A. Wixforth, Acoustically driven planar microfluidics, Superlattices Microstruct. **33**, 389 (2003).

[8] A. Renaudin, P. Tabourier, V. Zang, J. Camart, and C. Druon, Saw nanopump for handling droplets in view of biological applications, Sens. Actuators B **113**, 389 (2006).

[9] P. Brunet, M. Baudoin, O. B. Matar, and F. Zoueshtiagh, Droplet displacements and oscillations induced by ultrasonic surface acoustic waves: A quantitative study, Phys. Rev. E **81**, 036315 (2010).

[10] M. Baudoin, P. Brunet, O. Bou Matar, and E. Herth, Low energy droplet actuation via modulated surface acoustic waves, Appl. Phys. Lett. **100**, 154102 (2012).

[11] A. Bussonnière, M. Baudoin, P. Brunet, and O. Bou Matar, Dynamics of sessile and pendant drops excited by surface acoustic waves, Phys. Rev. E **93**, 053106 (2016).

[12] S. Shiokawa, Y. Matsui, and T. Ueda, Liquid streaming and droplet formation caused by leaky Rayleigh waves, IEEE Ultrason. Symp. **1**, 643 (1989).

[13] S. Shiokawa, Y. Matsui, and T. Ueda, Study on SAW streaming and its application to fluid device, Jpn. J. Appl. Phys. **29**, 137 (1990).

[14] K. Chono, N. Shimizu, Y. Matsui, J. Kondoh, and S. Shiokawa, Development of novel atomization system based on saw streaming, Jpn. J. Appl. Phys. **43**, 2987 (2004).

[15] A. Qi, L. Yeo, and J. Friend, Interfacial destabilization and atomization driven by surface acoustic waves, Phys. Fluids **20**, 074103 (2008).

[16] M. Tan, L. Yeo, and J. Friend, Rapid fluid flow and mixing induced in microchannelsusing surface acoustic waves, Europhys. Lett. **87**, 47003 (2009).

[17] M. Tan, J. Friend, and L. Yeo, Microparticle collection and concentration via a miniature surface acoustic wave device, Lab Chip **7**, 618 (2007).

[18] A. Rezk, L. Yeo, and J. Friend, Poloidal flow and toroidal particle ring formation in a sessile drop driven by megahertz order vibration, Langmuir **30**, 11243 (2014).

[19] T. Frommelt, M. Kostur, M. Wenzel-Schäfer, P. Talkner, P. Hänggi, and A. Wixforth, Microfluidic Mixing via Acoustically Driven Chaotic Advection, Phys. Rev. Lett. **100**, 034502 (2008).

[20] J. Kondoh, N. Shimizu, Y. Matsui, M. Sugimoto, and S. Shiokawa, Development of temperature control system for liquid droplet using surface acoustic wave device, Sens. Actuators A **149**, 292 (2009).

[21] J. Reboud, Y. Bourquin, G. Wilson, G. Pall, M. Jiwaji, A. Pitt, A. Graham, A. Waters, and J. Cooper, Shaping acoustic fields as a toolset for microfluidic manipulations in diagnostic technologies, Proc. Natl. Acad. Sci. USA **109**, 15162 (2012).

[22] R. J. Shilton, V. Mattoli, M. Travagliati, M. Agostini, A. Desii, F. Beltram, and M. Cecchini, Rapid and controllable digital microfluidic heating by surface acoustic waves, Adv. Funct. Mater. **25**, 5895 (2015).

[23] J. Blamey, L. Y. Yeo, and J. R. Friend, Microscale capillary wave turbulence excited by high frequency vibration, Langmuir **29**, 3835 (2013).

[24] A. Qi, J. R. Friend, L. Y. Yeo, D. A. Morton, M. P. McIntosh, and L. Spiccia, Miniature inhalation therapy platform using surface acoustic wave microfluidic atomization, Lab Chip **9**, 2184 (2009).

[25] A. Riaud, M. Baudoin, O. Bou Matar, J.-L. Thomas, and P. Brunet, On the influence of viscosity and caustics on acoustic streaming in sessile droplets: An experimental and a numerical study with a cost-effective method, J. Fluid Mech. **821**, 384 (2017).

[26] L. Rayleigh, On the capillary phenomena of jets, Proc. Roy. Soc. London **29**, 71 (1879).

[27] H. Lamb, *Hydrodynamics* (Cambridge University Press, Cambridge, 1932).

[28] A. Abramovici, W. Althouse, R. W. P. Drever, Y. Gursel, S. Kawamura, F. J. Raab, D. Shoemaker, L. Sievers, R. Spero, K. S. Thorne, R. E. Vogt, R. Weiss, S. E. Whitcomb, and M. Zucker, LIGO: The laser interferometer gravitational-wave observatory, Science **256**, 325 (1992).

[29] G. Jourdan, F. Comin, and J. Chevrier, Mechanical Mode Dependence of Bolometric Backaction in an Atomic Force Microscopy Microlever, Phys. Rev. Lett. **101**, 133904 (2008).

[30] I. Favero and K. Karrai, Optomechanics of deformable optical cavities, Nat. Photon. **3**, 201 (2009).

[31] C. Metzger, M. Ludwig, C. Neuenhahn, A. Ortlieb, I. Favero, K. Karrai, and F. Marquardt, Self-Induced Oscillations in an Optomechanical System Driven by Bolometric Backaction, Phys. Rev. Lett. **101**, 133903 (2008).

[32] A. Rezk, J. K. Tan, and L. Yeo, HYbriD Resonant Acoustics (HYDRA), Adv. Mater. **28**, 1970 (2016).

[33] See Supplemental Material at http://link.aps.org/supplemental/10.1103/PhysRevFluids.7.124201 for information on experiments, acoutic eigenmodes, droplet deformation imaging, unstable surface eigenmodes, and bistability of static droplet deformations, which includes Refs. [43–47].

[34] M. Baudoin and J.-L. Thomas, Acoustical tweezers for particle and fluid micromanipulation, Annu. Rev. Fluid Mech. **52**, 205 (2020).

[35] H. Li, J. R. Friend, and L. Y. Yeo, Microfluidic Colloidal Island Formation and Erasure Induced by Surface Acoustic Wave Radiation, Phys. Rev. Lett. **101**, 084502 (2008).

[36] J. Bostwick and P. Steen, Dynamics of sessile drops. Part 1. Inviscid theory, J. Fluid Mech. **760**, 5 (2014).

[37] E. M. Herrey, Experimental studies on acoustic radiation pressure, J. Acoust. Soc. Am. **27**, 891 (1955).

[38] F. E. Borgnis, Acoustic radiation pressure of planar compressional waves, Rev. Mod. Phys. **25**, 653 (1953).

[39] B. Issenmann, A. Auberon, R. Wunenburger, and J.-P. Delville, Acoustical spring effect in a compliant cavity, Eur. Phys. J. E **36**, 39 (2013).

[40] B. Issenmann, R. Wunenburger, S. Manneville, and J.-P. Delville, Bistability of a Compliant Cavity Induced by Acoustic Radiation Pressure, Phys. Rev. Lett. **97**, 074502 (2006).

[41] E. Mahravan, H. Naderan, and E. Damangir, Frequency and wavelength prediction of ultrasonic induced liquid surface waves, Ultrasonics **72**, 184 (2016).

[42] E. Mahravan, H. Naderan, and E. Damangir, Analysis of free surface oscillations of a droplet due to ultrasonic wave impingement, Phys. Fluids **32**, 092111 (2020).

[43] N. Gumerov and R. Duraiswami, *Fast Multipole Methods for the Helmholtz Equation in Three Dimensions* (Elsevier, Oxford, 2004).

[44] R. T. Frankot and R. Chellappa, A method for enforcing integrability in shape from shading algorithms, IEEE Trans. Pattern Anal. Machine Intell. **10**, 439 (1988).

[45] C.-T. Chang, J. Bostwick, S. Daniel, and P. Steen, Dynamics of sessile drops. Part 2. Experiment, J. Fluid Mech. **768**, 442 (2015).

[46] P. Bloomfield, *Fourier Analysis of Time Series: An Introduction* (John Wiley & Sons, New York, 2004).

[47] H. Chraïbi, D. Lasseux, E. Arquis, R. Wunenburger, and J.-P. Delville, Stretching and squeezing of sessile dielectric drops by the optical radiation pressure, Phys. Rev. E **77**, 066706 (2008).